Influence of graphene oxide's characteristics on the fabrication and performance of crosslinked nanofiltration membranes

Vepika Kandjou[a,b], *Zoraida González*[c], *Beatriz Acevedo*[a], *José M. Munuera*[c], *Juan I. Paredes*[c] *and Sonia Melendi-Espina*[a*]

[a] School of Engineering, University of East Anglia (UEA), Norwich Research park, NR4 7TJ, Norwich (UK)

[b] Department of Chemical, Materials and Metallurgical Engineering (CMME), Botswana International University of Science and Technology (BIUST), P/Bag 16, Palapye, (Botswana)

[c] Instituto de Ciencia y Tecnología del Carbono (INCAR-CSIC), C/ Francisco Pintado Fe 26, 33011, Oviedo (Spain)

ABSTRACT

Graphene oxide (GO) is emerging as an excellent next generation material for water purification membranes. Its ability to be fabricated cost-effectively in large quantities and featured characteristics, such as hydrophilicity, makes it an equitable graphene alternative in respective nanometric applications, including nanofiltration. In this study, the influence of key properties of the GO sheets, such as lateral size, surface chemistry and colloid stability, on the successful fabrication and subsequent water purification performance of crosslinked nanofiltration membranes is analysed. GO water suspensions with nanosheets of different lateral sizes and distribution of oxygenated functional groups were prepared by controlling the

sonication time (from 0 to 180 minutes) starting from commercial GO. The variation of the physicochemical characteristics of the resulting GO sheets was comprehensively studied by means of atomic force microscopy, UV-Vis absorption spectroscopy, zeta potential measurements and X-Ray photoelectron spectroscopy. The morphology of the subsequently fabricated membranes was hereafter examined via scanning electron microscopy, while their nanofiltration performance was investigated against methylene blue solution. The influence of GO's physicochemical characteristics on membrane performance was apparent, with the average rejection values ranging from 59.8% to 98.4% at a changing lateral size and surface chemistry.

KEYWORDS

Graphene oxide, lateral size, surface chemistry, cross-linked membranes, water purification, nanofiltration

[1].

- *Corresponding author: Sonia Melendi-Espina; s.melendi-espina@uea.ac.uk; Telephone: +441603592848*

1. Introduction

The changing global climate, depletion of underground water aquifers together with the exponential increase in human population heightens the impending global water shortage [1–3]. Correspondingly, there is an urgent need for the implementation and optimisation of cutting-edge, durable and efficient water purification membrane materials [4,5]. Several carbon-based materials, from multi walled carbon nanotubes to activated carbons, are suitable candidates in the fabrication of notable next generation water purification and treatment frameworks [6–9], and at the forefront of these promising materials is graphene [10]. However, despite its excellent properties, such as mechanical stability and mono-atomic thickness [11], the lack of suitable large-scale production strategies is hampering its wide use in commercial applications [12–15]. In this context, graphene oxide (GO) arises as a very promising graphene substitute due to its ability to be cost effectively fabricated from graphite [16–18]. Though not mechanically as strong as graphene, the presence of oxygenated functional groups on its surface lends hydrophilicity, which strengthen its potential use as a water purification membrane material [19–21]. Moreover, thin GO films advantageously offer a unique tortuous water flow channel that is responsible for a faster water flow relative to other nanomaterials [22].

Nevertheless, a prevailing problem in the use of GO as a water purification membrane is the membrane swelling phenomenon, where the membrane pore gap widens as a result of the accumulation of water molecules onto its hydrophilic oxygenated functional groups [23–25]. Thus far, several efforts have been undertaken to alleviate this problem. For instance, Huang *et al*. explored the use of reduced GO, which has diminished oxygenated functional groups, hence limiting the entrapment of water molecules [26]. However, the loss of membrane hydrophilicity comes with the need of a higher operation pressure and increased membrane susceptibility to fouling [27–29]. Other approaches, such as the incorporation of crosslinkers,

have been also explored to control the inter-flake gap and in this way optimising permeation abilities [19].

Despite crosslinkers having been previously demonstrated to enhance GO membrane nanofiltration performance and stability [19], little is known about the influence of the physicochemical characteristics of the GO used as starting material on both membrane fabrication and their behaviour in water purification. Elsewhere it has been noted that some GO characteristics, particularly its lateral size and surface chemistry, determine its efficiency in potential applications [30]. For instance, Kim *et al*. observed that properties of GO nanocomposites, such as dispersing ability and mechanical strength, are strongly dependent on its lateral size [31].

It is therefore key to understand the impact of diverse GO characteristics on the quality, morphology and subsequent performance of crosslinked nanofiltration membranes. There are also theoretical simulations and experimental studies evaluating the impact of the synthesis conditions on the physicochemical and transport characteristics of GO laminates [32], as well as the influence of GO sheet lateral size on water permeance of GO pressure-assisted membranes [33]. However, to the best of our knowledge, there are no studies simultaneously investigating the effect of GO lateral size, its surface chemistry and colloidal stability on the crosslinked membranes' fabrication procedure and their nanofiltration performance.

For this purpose, different aqueous GO suspensions were produced from the same raw material by varying the sonication time. GO layers with different average lateral size and type/distribution of oxygenated functional groups were obtained, which generate cross-linked membranes with notable differences in terms of morphology and behaviour in nanofiltration.

2. Experimental section

2.1 Reagents

GO powder (product code: C889/GOB019/Pw2) was commercially sourced from Graphenea Co. (Spain), while p-phenylenediamine powder (PPD, product code: P6001), polyethyleneimine (PEI, product code 03880), potassium hydroxide powder (KOH) and methylene blue (MB, $C_{16}H_{18}ClN_3S.3H_2O$, >99% purity; product code: M9140) were purchased from Sigma Aldrich (UK). 0.2 μm pore sized, 47 mm diameter fibrous poly (acrylonitrile) (PAN) filter substrates were supplied by Sterlitech Corporations in Washington DC, (USA).

2.2 Preparation of GO suspensions

A GO suspension of 0.5 mg/ml (GO-0') was prepared by mild mechanical agitation of the corresponding amount of commercial GO powder in deionised water. Then, four aliquots of the parent sample were sonicated for different times (30, 60, 120 and 180 minutes) by means of a 280 W sonication power bath-type sonicator operated at a frequency of 55 Hz (Fisherbrand FB1505, Elmasonic S30H). The samples were labelled as GO-X', with X denoting the corresponding sonication time.

2.3 Sample characterisations

2.3.1 Atomic Force Microscopy (AFM)

The lateral size and the height profiles of the different GO samples were measured using AFM imaging and profiling by depositing a drop (~50 μl) of a water suspension of each sample onto a highly oriented pyrolytic graphite (HOPG) substrate that was pre-heated at ~50-60 ºC. The GO sheets were imaged using a Nanoscope IIIa Multimode (Veeco Instruments) operating in tapping mode under ambient conditions. Silicon cantilevers having resonance frequency and spring constant of 250-300 kHz and ~40 N m^{-1} were used. The images were processed and

analysed using Scanning Probe Image Processor (SPIP) software to estimate the average lateral sizes from several sections of the respective GO samples.

2.3.2 UV-Vis spectra measurements

UV-Vis spectra measurements (Hitachi U-3900 UV-Vis) of the respective suspensions were undertaken and respective calibration lines were constructed. This was done to calculate each sample's absorption coefficients (α_{GO}) based on the Lambert-Beer law (Eq.1). The coefficient is a lateral size dependent parameter [34].

$$A = \alpha_{GO}.c.l \qquad \text{Eq. 1}$$

Where A, the absorbance (a.u.), is a product of the absorbance coefficient, α_{GO}, the concentration, c (mg/ml), and the optical path length, l (m), (length that the light passes through during UV-Vis measurements, cuvette length (0.01 m)).

2.3.3 X-ray Photoelectron Spectroscopy measurements

The surface chemistry of the different GO samples was evaluated by X-ray Photoelectron Spectroscopy (XPS) measurements (Kratos Axis Ultra-DLD, K-Alpha^{+}). Each suspension (GO-0' - GO-180') was centrifuged in a Bio-Fuge Primo Heraeus centrifuge (1000 rpm for 10 minutes) to collect samples for characterisation.

The bonding type and functional groups present in the samples (mainly, the oxygen functional groups) were estimated by curve fitting the C1s and O1s spectra using a Gaussian- Lorentzian peak shape, after performing a Shirley background correction. The major peaks for the C1s curve were the C graphitic (Binding energy, BE, = 284.3–284.4 eV), C-O epoxide/C-OH hydroxyl (BE = 285.6–285.7 eV), C=O carbonyl (BE = 286.9-287.0 eV), as well as the O-C=O carboxyl (B.E = 288.9 eV) and the π-π* shake-up signal (290.8 eV) that is typical for sp^2 hybridized carbon. However it is important to note that overlap of oxygen functionalities, specifically between C(epoxy) and hydroxyls, was notable [35–37]. For the high-resolution O

1s curve fittings, 5 major peaks similarly emerged, representing the (C=O) carbonyl, (C=O) carboxyl, (C-OH) hydroxyl, (C-O) epoxy and (C-O) carboxylic groups respectively [38].

2.3.4 Zeta (ζ) potential measurements

To investigate the GO suspension stability and dispersibility of the nanosheets at a changing lateral size, ζ - potential measurements were undertaken using a Zetasizer Nano series (Nano ZS90, Malvern, UK) for a quantifiable relation.

2.3.5 Membrane fabrication, characterisation and performance tests

The membrane fabrication via layer-by-layer assembly has been described in detail in previous works [19,39]. A rotary dip coater (ND-R 11/2, S/N: 522016) (Nadetech Innovations, Navarra, Spain) was used to alternatively immerse the pre-treated PAN substrates in the corresponding GO suspensions and PPD solutions. The fabricated crosslinked membranes were accordingly labelled as M-GO-X' (with X being the time of sonication of the GO suspension used as starting material). A dipping immersion time of 1 minute was entailed and 5 bi-layers of GO-PPD were assembled for each membrane type.

Membrane morphology was analysed by means of a JEOL JSM – 5900 LV Scanning Electron Microscope (SEM). Membrane performance tests were then evaluated with a pressure-assisted nanofiltration of 10 mg/l aqueous solution of methylene blue (MB). 100 ml of MB solution was passed through each membrane at an operation pressure of 1 bar in order to determine the flux and dye rejection across the membrane [19]. Three membranes of each GO sample type were fabricated and tested; thus, to enhance the reliability of the results, the average of three measured rejections and fluxes were taken, noting down the standard deviation in error bars.

3. Results and discussion

3.1 Physicochemical characteristics of GO.

The average lateral size of the GO sheets, as evaluated by means of AFM, diminishes significantly with an increase in sonication time (Figure 1). The decrease is more significant after the first 60 minutes, leading to approximately 45% reduction of the average lateral size. Successive increases in the sonication time (up to 180 minutes) are not as effective in reducing the GO size. These results are in qualitative consonance with previous literature, where an exponential decay in GO nanosheet size with sonication has been reported [40,41].

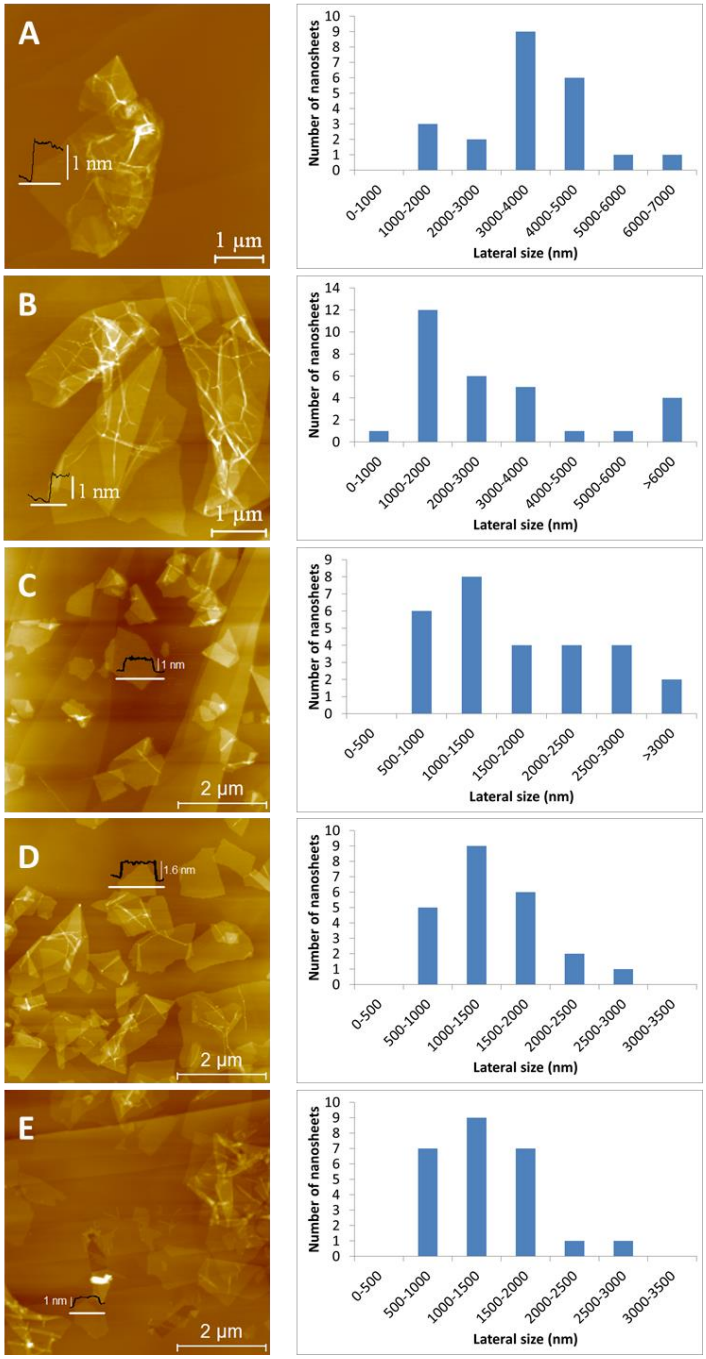

Figure 1. AFM images of the differently sonicated samples; A) GO-0' B) GO-30' C) GO-60' D) GO-120' and E) GO-180' and their respective histograms depicting their lateral size distribution.

Besides boasting larger nanosheets, GO-0' and GO-30' also show a wider size distribution, containing sheets with lateral dimensions above 4 µm, which are not present in samples sonicated for longer periods (Figure 1). Additionally, and regardless of their dimensions, the

majority of the GO sheets tend to be mono layer, as observed from the height profiles in Figure 1 [42].

The samples were further examined via UV-Vis absorption spectroscopy. Though a cumulative combination of factors (such as the number of layers and surface chemistry) also affect UV-Vis absorbance, GO lateral-size is a key factor [43]. The absorbance of suspensions has been quantified by the determination of the absorbance coefficient (α) using the Lambert-Beer law (Eq. 1) [34]. The coefficient has been determined at 660 nm, because it is noted in literature that at this wavelength there is minimal interference on absorbance from GO's chemical functionalities, and hence absorbance is predominantly a function of the lateral size [44].

It has been reported that suspensions containing smaller GO sheets may increase light absorption [43], which is in agreement with our findings, as an inverse relation between the absorbance coefficient and lateral size has been found (Figure 2). The optical absorbance in the visible region is enhanced with the sonication time, increasing the absorption coefficient from 670 to 830 ml mg^{-1} m^{-1}.

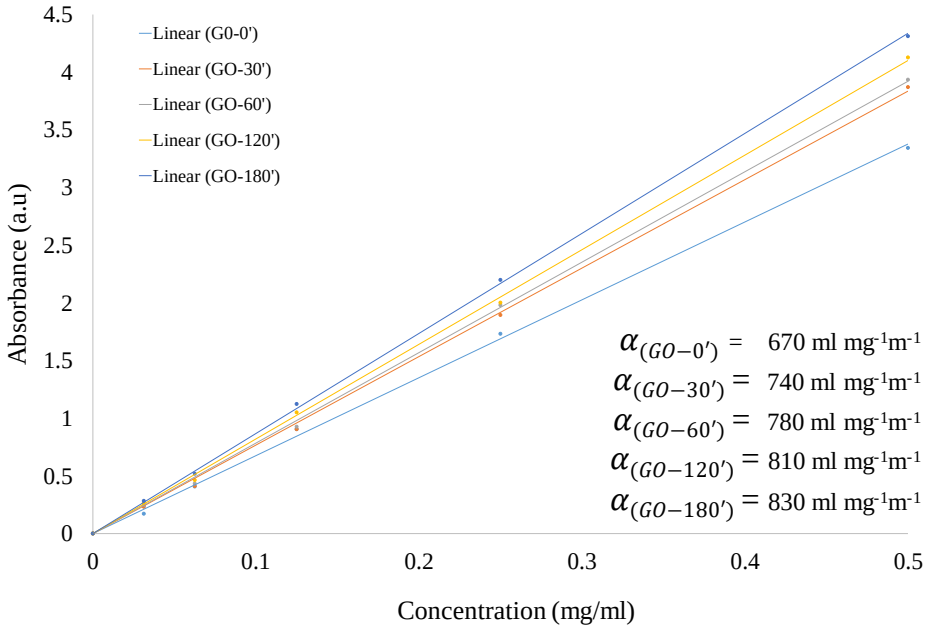

Figure 2. Absorbance coefficients of the prepared samples.

The decrease in GO lateral size with sonication time is also accompanied by noticeable changes in the surface chemistry, mainly in terms of type, amount and distribution of oxygen functional groups (Table 1).

Table 1. Surface chemistry of GO samples determined by XPS (at. %)

	GO-0'	**GO-30'**	**GO-60'**	**GO-120'**	**GO-180'**
C 1s curve					
C1s (%)	71.2	67.9	67.6	68.8	68.1
O1s (%)	27.4	31.3	31.4	31.5	31.2
C/O (%)	2.6	2.3	2.2	2.2	2.2
Csp^2+Csp^3 (%)	58.0	42.5	44.0	43.4	45.4
C-O Hydroxyl/Epoxy (%)	36.6	50.1	44.7	42.6	39.2
C=O Carbonyl (%)	1.2	1.7	5.8	7.7	9.0
COOH Carboxyl (%)	4.2	4.7	4.5	5.0	5.4
π *-π*	0.0	1.0	1.0	1.3	1.0
O 1s curve					
C=O Carbonyl (%)	8.8	10.0	10.8	12.2	14.4
C=O Carboxyl (%)	3.2	5.3	6.5	7.6	9.4
C-O Hydroxyl (%)	54.4	49.7	47.9	45.5	40.3
C-O Epoxy (%)	30.4	29.7	28.3	27.1	26.5
C-O Carboxyl (%)	3.2	5.3	6.5	7.6	9.4

A notable drop in abundance of the overlapping basal plane functional groups (hydroxyls and epoxy groups) is observed as the lateral size decreases (Table 1). Although there is still ambiguity in processes that lead to the sonication fragmentation of GO at the atomistic level, Li *et al.* proposed that cooperatively aligned epoxy groups initiate fragmentations in GO with prolonged sonication [45]. As such, their abundance decreases with lessening in nanosheet lateral size during fragmentation.

On the other hand, carbonyl and carboxylic groups are located at the edges of the GO sheets, as in accordance to the Lerf–Klinowski model [46]. Thus, as nanosheets fragment, the cumulative peripheral area increases as well as the presence of these types of oxygen functionalities (Table 1), which can be beneficial for the MB rejection, as it is a cationic dye [47].

The increase in the prevalence of the oxygenated groups located at the sheet edges is accompanied by an improvement in suspension stability [48,49], which is reflected on the zeta potential of the samples. Zeta potential is equivalent to the degree of electrostatic repulsions between adjacent nanoparticles/nanosheets and therefore it is an important parameter to quantify both dispersibility and stability of colloidal samples [49,50]. The zeta potential increases (in absolute value) from -18.1 to -34.8 mV as the GO lateral size decreases (Table 2). GO-0' and GO-30' are categorized as incipiently unstable, meaning they tend to flocculate and agglomerate (which was indeed the case for GO-0´) after standing undisturbed for several days, while GO-60', GO-120' and GO-180', with electrostatic repulsion above ±30 mV (absolute value), are inherently stable [51,52].

Table 2. Zeta potential of the GO suspensions

Sample	**ζ (mV)**
GO-0'	-18.1
GO-30'	-25.0
GO-60'	-32.5
GO-120'	-34.0
GO-180'	-34.8

3.2 Influence of the starting GO on the subsequent membrane characteristics

As aforementioned, GO samples obtained at different sonication times were used for the fabrication of a variety of membranes. A darker pigmentation of the membranes from M-GO-0' to M-GO-180' can be observed (Figure 3). GO is dark-brownish in colour and therefore an increase in its accumulation onto the substrates during fabrication leads to a darkening in pigmentation of the membranes. This might be due to an improved interaction between GO and PPD during the layer-by-layer assembly, which is promoted by the enhanced stability of the samples with time of sonication and with the type and distribution of GO functional groups [53], as demonstrated by zeta potential measurements shown in Table 2.

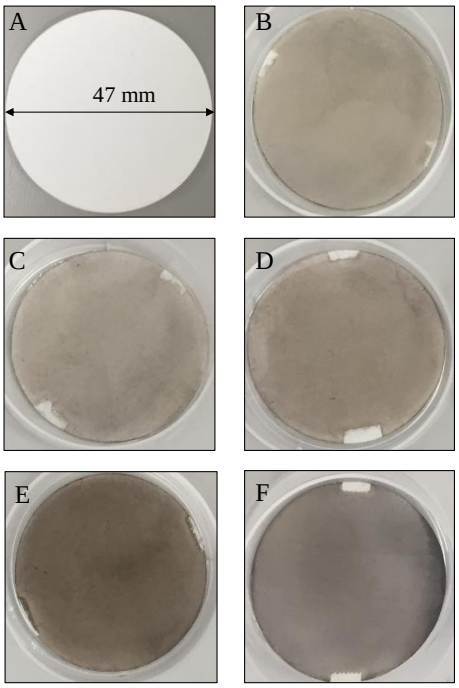

Figure 3. Images of the fabricated membranes; A) plain PAN substrate, B) M-GO-0’ C) M-GO-30’, D) M-GO-60’, E) M-GO-120’ F) M-GO-180’.

The membrane morphology was investigated by means of SEM, including the plain PAN supporting substrate for comparative purposes (Figure 4). As it can be observed, M-GO-0’ exhibits evident discontinuity in covering the substrate, as notches of PAN fibres are clearly visible (Figure 4B). This result could be explained considering the lack of appropriate suspension stability of the GO sheets in sample GO-0´, as depicted by its low zeta potential (-18.1 mV, Table 2). On the other hand, membranes from M-GO-30’ to M-GO-180’ show a homogeneous coverage of the substrate with highly reduced presence of visible PAN fibres (Figures 4C-F), which is in agreement with their improved colloidal/suspension stability.

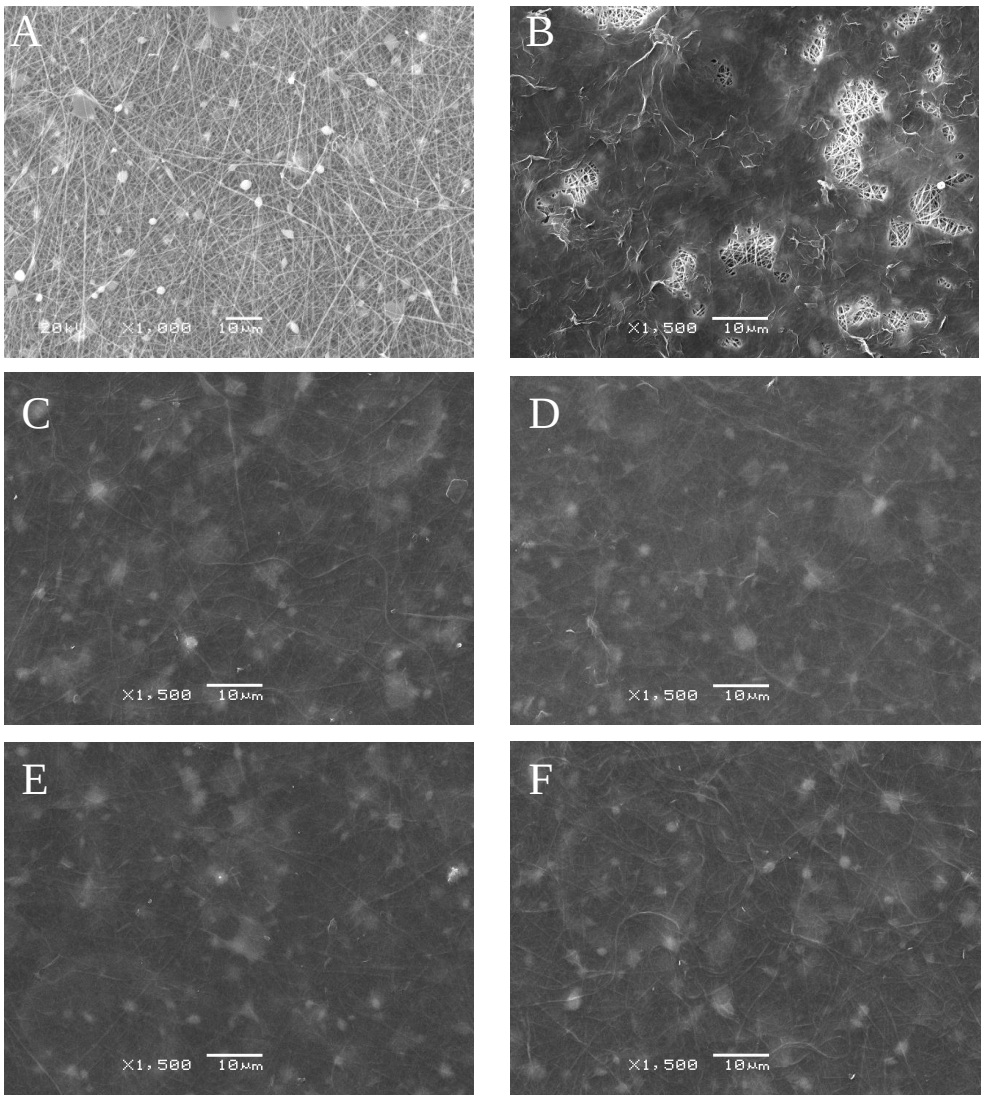

Figure 4. SEM images of A) plain PAN substrate, B) M-GO-0' C) M-GO-30', D) M-GO-60', E) M-GO-120'and F) M-GO-180'.

3.3 Membrane performance analysis

3.3.1 Membrane rejection

The MB nanofiltration results indicate that membrane performance significantly increases as the GO lateral size decreases and the presence of peripheral oxygen groups rises. The average rejection increases from 59.8 to 93.9 % when evaluating the behaviour of M-GO-0´and M-GO-30´, respectively (Figure 5). Plateauing in performance post M-GO-60' with an average increased elimination of 97.8% ± 0.6% was observed (Figure 5). These results are in correlation

with the previous ones, thus corroborating the influence of membranes homogeneity on their rejection. The good colloidal stability of GO-60', GO-120' and GO-180' (i.e. the higher amount of individual GO sheets in these suspensions) is mainly due to their optimum lateral size and the type/distribution of oxygen functional groups (e.g., increased fraction of edges with ionizable oxygen groups), which also enhance the adsorption of MB (cationic dye) due to the electrostatic attraction [54]. Furthermore, in our previous work, a physisorption ($\pi - \pi$ interactions) separation mechanism between GO´s non oxidised regions and MB was noted, also positively contributing to the improvement in membrane rejection [19]. The favourability of small flake GO nanosheets over large flake in organic dye nanofiltration has also recently been reported elsewhere [55].

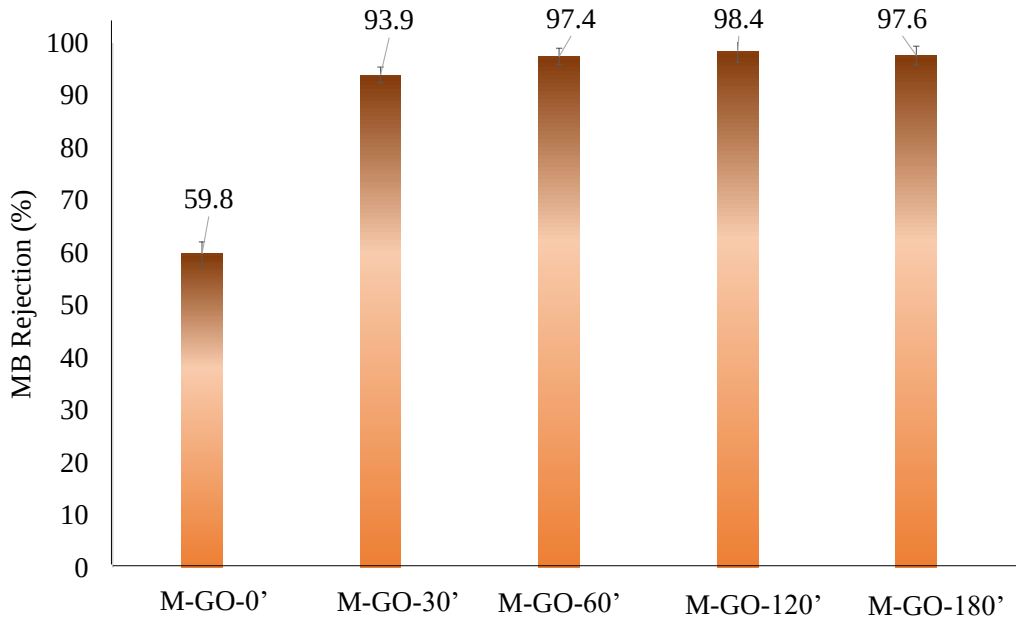

Figure 5. MB rejection results of the membranes with respective permeate solutions

3.3.2 Permeation flux across the membranes

The flux counters the rejection results, as the higher the flux, the lower the rejection. For M-GO-0' a very high flux of 890.7 l/m^2.h was recorded (Figure 6). This is evidently due to the

lack of uniform coverage of this membrane (Figure 4B). The large notches in the areas of no coverage are the likely reason for the observed high flux and low rejection. Membrane continuity and homogeneity are thus significant properties in membrane separation performance [19]. The impact of membrane homogeneity, or its lack of, it is therefore likely to be apparent in membrane rejection, flux and other significant membrane characteristics as observed.

Fluxes in the 3.6 – 5.5 $l/m^2.h$ range were subsequently recorded for the M-GO-60' to M-GO-180' membranes, owing to excellent membrane homogeneity and intactness.

Although M-GO-30' shows an appropriate morphology (Figure 4C), it rejects MB less efficiently and the flow across this membrane is higher than that for M-GO-60', M-GO-120' and M-GO-180'. This might be due to the somewhat inferior colloidal stability of the parent sample GO-30', which presents a zeta potential below the ±30mV threshold established for a stable suspension (Table 2). When they possess a better dispersibility, more GO nanosheets are exposed for better crosslinking with PPD via an epoxy ring opening reaction [19]. The resulting more homogeneous and stable membranes show an enhanced performance hence the declining flux as claimed by Wei *et al* [56].

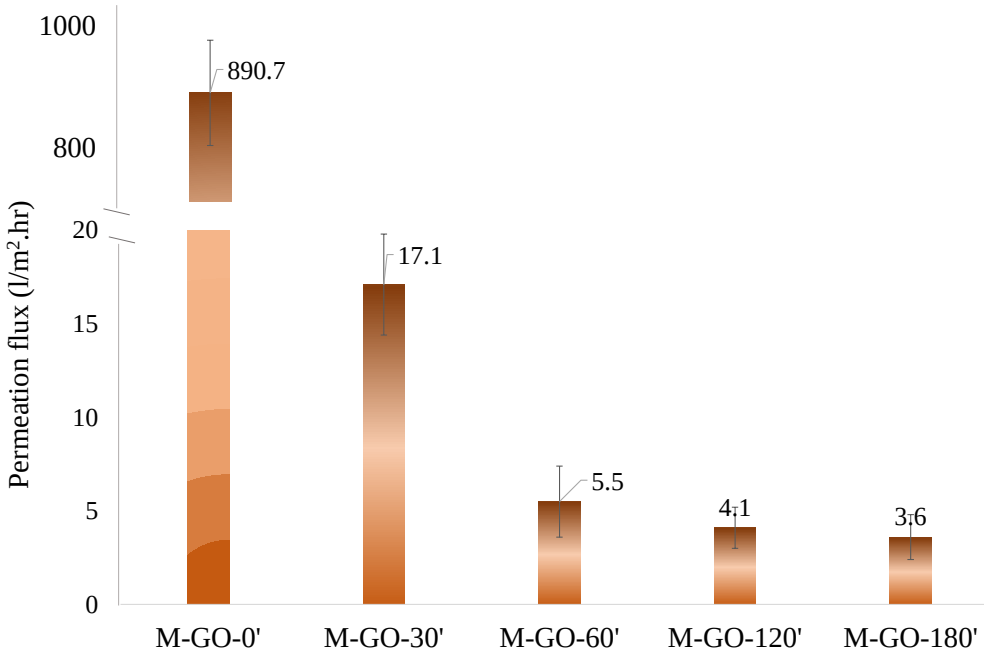

Figure 6. Permeation flux of the fabricated membranes

4. Conclusions

The interdependence of the lateral size and surface chemistry of GO sheets appears to be key in the nanofiltration performance of cross-linked GO membranes. In consequence, controlling important GO characteristics, such as average lateral size and type/amount of oxygenated functional groups, is significant in membranes quality and performance. The different physicochemical characteristics achieved when tuning synthesis parameters, e.g. sonication time, influence not only the stability of the GO sheets, but also the effectiveness of the crosslinking mechanism and, subsequently, the nanofiltration performance of the resulting membranes. GO sheets obtained at sonication times longer than 60 minutes show a suitable lateral size and an appropriate amount of COOH functional groups, located at the edges, to enhance the removal of cationic dyes, reaching rejection values greater than 97 %.

Acknowledgments

V.K. special gratitude to the Botswana Government's Top Achievers Scholarship Programme for the scholarship (TR.163096). J.M.M. and J.I.P. acknowledge funding from the Spanish

Ministerio de Ciencia, Innovación y Universidades (MICINN), Agencia Estatal de Investigación (AEI) and the European Regional Development Fund (ERDF) through project RTI2018-100832-B-I00.

References

[1] M. Kummu, J.H.A. Guillaume, H. De Moel, S. Eisner, M. Flörke, M. Porkka, The world ' s road to water scarcity : shortage and stress in the 20th century and pathways towards sustainability, Nat. Publ. Gr. (2016) 1–16. https://doi.org/10.1038/srep38495.

[2] S.N. Gosling, N.W. Arnell, A global assessment of the impact of climate change on water scarcity, Clim. Change. 134 (2016) 371–385. https://doi.org/10.1007/s10584-013-0853-x.

[3] J. Schewe, J. Heinke, D. Gerten, I. Haddeland, N.W. Arnell, D.B. Clark, R. Dankers, S. Eisner, B.M. Fekete, F.J. Colón-González, S.N. Gosling, H. Kim, X. Liu, Y. Masaki, F.T. Portmann, Y. Satoh, T. Stacke, Q. Tang, Y. Wada, D. Wisser, T. Albrecht, K. Frieler, F. Piontek, L. Warszawski, P. Kabat, Multimodel assessment of water scarcity under climate change, Proc. Natl. Acad. Sci. 111 (2014) 3245–3250. https://doi.org/10.1073/pnas.1222460110.

[4] N.L. Le, S.P. Nunes, Materials and membrane technologies for water and energy sustainability, Sustain. Mater. Technol. 7 (2016) 1–28. https://doi.org/10.1016/j.susmat.2016.02.001.

[5] S. Chisca, P.H.H. Duong, A.H. Emwas, R. Sougrat, S.P. Nunes, Crosslinked copolyazoles with a zwitterionic structure for organic solvent resistant membranes, Polym. Chem. 6 (2015) 543–554. https://doi.org/10.1039/c4py01293c.

[6] X. Liu, M. Wang, S. Zhang, B. Pan, Application potential of carbon nanotubes in water treatment: A review, J. Environ. Sci. (China). 25 (2013) 1263–1280.

https://doi.org/10.1016/S1001-0742(12)60161-2.

[7] R. Das, M.E. Ali, S.B.A. Hamid, S. Ramakrishna, Z.Z. Chowdhury, Carbon nanotube membranes for water purification: A bright future in water desalination, Desalination. 336 (2014) 97–109. https://doi.org/10.1016/j.desal.2013.12.026.

[8] M. Elimelech, W.A. Phillip, The Future of Seawater Desalination: Energy, Technology and the Environment, Science (80-.). 333 (2011) 712–718. https://doi.org/10.1126/science.1200488.

[9] J.R. Werber, C. Osugi, M. Elimeneck, Materials for next-generation desalination and water purification membranes, Nat. Mater. 1 (2016). https://doi.org/10.1038/natrevmats.2016.18.

[10] S. Homaeigohar, M. Elbahri, Graphene membranes for water desalination, NPG Asia Mater. 9 (2017) e427. https://doi.org/10.1038/am.2017.135.

[11] H. Chen, M.B. Müller, K.J. Gilmore, G.G. Wallace, D. Li, Mechanically strong, electrically conductive, and biocompatible graphene paper, Adv. Mater. 20 (2008) 3557–3561. https://doi.org/10.1002/adma.200800757.

[12] L. Dong, Z. Chen, X. Zhao, J. Ma, S. Lin, M. Li, Y. Bao, L. Chu, K. Leng, H. Lu, K.P. Loh, A non-dispersion strategy for large-scale production of ultra-high concentration graphene slurries in water, Nat. Commun. 9 (2018) 1–8. https://doi.org/10.1038/s41467-017-02580-3.

[13] A. Zurutuza, C. Marinelli, Challenges and opportunities in graphene commercialization, Nat. Nanotechnol. 9 (2014) 730–734. https://doi.org/10.1038/nnano.2014.225.

[14] C. Nethravathi, M. Rajamathi, Chemically modified graphene sheets produced by the solvothermal reduction of colloidal dispersions of graphite oxide, Carbon N. Y. 46

(2008) 1994–1998. https://doi.org/10.1016/j.carbon.2008.08.013.

[15] L.Y. Zhong, Z. Tian, G.P. Simon, D. Li, Scalable production of graphene via wet chemistry: progress and challenges, Mater. Today. 18 (2015) 73–78. https://doi.org/10.1016/j.mattod.2014.08.019.

[16] W.S. Hummers, R.E. Offeman, Preparation of Graphitic Oxide, J. Am. Chem. Soc. 80 (1958) 1339. https://doi.org/10.1021/ja01539a017.

[17] J. Ma, D. Ping, X. Dong, Recent developments of graphene oxide-based membranes: A review, Membranes (Basel). 7 (2017). https://doi.org/10.3390/membranes7030052.

[18] Y. Zhu, S. Murali, W. Cai, X. Li, J.W. Suk, J.R. Potts, R.S. Ruoff, Graphene and graphene oxide: Synthesis, properties, and applications, Adv. Mater. 22 (2010) 3906–3924. https://doi.org/10.1002/adma.201001068.

[19] V. Kandjou, A.M. Perez-mas, B. Acevedo, M. Hernaez, A.G. Mayes, S. Melendi-espina, Enhanced covalent p-phenylenediamine crosslinked graphene oxide membranes : Towards superior contaminant removal from wastewaters and improved membrane reusability, J. Hazard. Mater. 380 (2019) 120840. https://doi.org/10.1016/j.jhazmat.2019.120840.

[20] T.Z. Shen, S.H. Hong, J.K. Song, Electro-optical switching of graphene oxide liquid crystals with an extremely large Kerr coefficient, Nat. Mater. 13 (2014) 394–399. https://doi.org/10.1038/nmat3888.

[21] D. Chen, H. Feng, J. Li, Graphene oxide: Preparation, functionalization, and electrochemical applications, Chem. Rev. 112 (2012) 6027–6053. https://doi.org/10.1021/cr300115g.

[22] R.. Nair, H.. Wu, A. V. Jayaram, V. Grigorieva, A.. Geim, Unimpeded Permeation of Water Through Helium-Leak–Tight Graphene-Based Membranes, Science (80-.). 335

(2012) 442–445. https://doi.org/10.1126/science.1211694.

[23] W.S. Hung, C.H. Tsou, M. De Guzman, Q.F. An, Y.L. Liu, Y.M. Zhang, C.C. Hu, K.R. Lee, J.Y. Lai, Cross-linking with diamine monomers to prepare composite graphene oxide-framework membranes with varying d-spacing, Chem. Mater. 26 (2014) 2983–2990. https://doi.org/10.1021/cm5007873.

[24] S. Zheng, Q. Tu, J.J. Urban, S. Li, B. Mi, Swelling of Graphene Oxide Membranes in Aqueous Solution: Characterization of Interlayer Spacing and Insight into Water Transport Mechanisms, ACS Nano. 11 (2017) 6440–6450. https://doi.org/10.1021/acsnano.7b02999.

[25] A. Klechikov, J. Yu, D. Thomas, T. Sharifi, A. V. Talyzin, Structure of graphene oxide membranes in solvents and solutions, Nanoscale. 7 (2015) 15374–15384. https://doi.org/10.1039/c5nr04096e.

[26] L. Huang, J. Chen, T. Gao, M. Zhang, Y. Li, L. Dai, L. Qu, G. Shi, Reduced Graphene Oxide Membranes for Ultrafast Organic Solvent Nanofiltration, Adv. Mater. 28 (2016) 8669–8674. https://doi.org/10.1002/adma.201601606.

[27] J. Wang, X. Gao, H. Yu, Q. Wang, Z. Ma, Z. Li, Y. Zhang, C. Gao, Accessing of graphene oxide (GO) nanofiltration membranes for microbial and fouling resistance, Sep. Purif. Technol. 215 (2019) 91–101. https://doi.org/10.1016/j.seppur.2019.01.018.

[28] F. Perreault, M.E. Tousley, M. Elimelech, Thin-Film Composite Polyamide Membranes Functionalized with Biocidal Graphene Oxide Nanosheets, Environ. Sci. Technol. Lett. 1 (2013) 71–76. https://doi.org/10.1021/ez4001356.

[29] S. Liu, T.H. Zeng, M. Hofmann, E. Burcombe, J. Wei, R. Jiang, J. Kong, Y. Chen, Antibacterial activity of graphite, graphite oxide, graphene oxide, and reduced graphene oxide: Membrane and oxidative stress, ACS Nano. 5 (2011) 6971–6980.

https://doi.org/10.1021/nn202451x.

[30] C. Botas, P. Álvarez, P. Blanco, M. Granda, C. Blanco, R. Santamaria, L.J. Romasanta, R. Verdejo, M.A. Lopez-Manchado, R. Menéndez, Graphene materials with different structures prepared from the same graphite by the Hummers and Brodie methods, Carbon N. Y. 65 (2013) 156–164. https://doi.org/10.1016/j.carbon.2013.08.009.

[31] J. Kim, S.W. Kim, H. Yun, B.J. Kim, Impact of size control of graphene oxide nanosheets for enhancing electrical and mechanical properties of carbon nanotube-polymer composites, RSC Adv. 7 (2017) 30221–30228. https://doi.org/10.1039/c7ra04015f.

[32] A. Paneri, S. Moghaddam, Impact of synthesis conditions on physicochemical and transport characteristics of graphene oxide laminates, Carbon N. Y. 86 (2015) 245–255. https://doi.org/10.1016/j.carbon.2015.01.024.

[33] V. Saraswat, R.M. Jacobberger, J.S. Ostrander, C.L. Hummell, A.J. Way, J. Wang, M.T. Zanni, M.S. Arnold, Invariance of water permeance through size-differentiated graphene oxide laminates, ACS Nano. 12 (2018) 7855–7865. https://doi.org/10.1021/acsnano.8b02015.

[34] M. Lotya, P.J. King, U. Khan, S. De, J.N. Coleman, High-concentration, surfactant-stabilized graphene dispersions, ACS Nano. 4 (2010) 3155–3162. https://doi.org/10.1021/nn1005304.

[35] A.P. Dementjev, A. de Graaf, M.C.. van de Sanden, A.. Maslakov, K.I Naumkin, A.. Serov, X-Ray photoelectron spectroscopy reference data for identification of the C3 N4 phase in carbon-nitrogen films., Diam. Relat. Mater. 9 (2000) 1904–1907. https://doi.org/10.1016/S0925-9635(00)00345-9.

[36] S. Bhattacharyya, C. Cardinaud, G. Turban, Spectroscopic determination of the structure of amorphous nitrogenated carbon films, J. Appl. Phys. 83 (1998) 4491.

[37] S. Bhattacharyya, J. Hong, G. Turban, Determination of the structure of amorphous nitrogenated carbon films by combined Raman and x-ray photoemission spectroscopy, J. Appl. Phys. 83 (1998) 3917. https://doi.org/10.1063/1.367312.

[38] Y.C.G. Kwan, G.M. Ng, C.H.A. Huan, Identification of functional groups and determination of carboxyl formation temperature in graphene oxide using the XPS O 1s spectrum, Thin Solid Films. 590 (2015) 40–48. https://doi.org/10.1016/j.tsf.2015.07.051.

[39] V. Kandjou, M. Hernaez, B. Acevedo, S. Melendi-espina, Interfacial crosslinked controlled thickness graphene oxide thin- fi lms through dip-assisted layer-by-layer assembly means, Prog. Org. Coatings. 137 (2019). https://doi.org/10.1016/j.porgcoat.2019.105345.

[40] S. Kumar, A. Garg, A. Chowdhuri, Sonication effect on graphene oxide (GO) membranes for water purification applications, Mater. Res. Express. 6 (2019). https://doi.org/10.1088/2053-1591/ab1ffd.

[41] A.F. Rodrigues, L. Newman, N. Lozano, S.P. Mukherjee, B. Fadeel, C. Bussy, K. Kostarelos, A blueprint for the synthesis and characterisation of thin graphene oxide with controlled lateral dimensions for biomedicine, 2D Mater. 5 (2018). https://doi.org/10.1088/2053-1583/aac05c.

[42] P. Solís-Fernández, J.I. Paredes, S. Villar-Rodil, A. Martínez-Alonso, J.M.D. Tascón, Determining the thickness of chemically modified graphenes by scanning probe microscopy, Carbon N. Y. 48 (2010) 2657–2660. https://doi.org/10.1016/j.carbon.2010.03.033.

[43] M. Hashemi, B. Muralidharan, M. Omidi, J. Mohammadi, Y. Sefidbakht, E.S. Kima, H.D.C. Smyth, M. Shalbaf, T.E. Milner, Effect of size and chemical composition of graphene oxide nanoparticles on optical absorption cross-section, J. Biomed. Opt. 23 (2018) 1. https://doi.org/10.1117/1.jbo.23.8.085007.

[44] S. Pandit, M. De, Empirical Correlation and Validation of Lateral Size-Dependent Absorption Coefficient of Graphene Oxides, ChemistrySelect. 2 (2017) 10004–10009. https://doi.org/10.1002/slct.201701893.

[45] J.-L. Li, K.K. Kudin, M.J. McAllister, R.K. Prud'homme, I.A. Aksay, R. Car, Oxygen-Driven Unzipping of Graphitic Materials, Infect. Immun. 96 (2006) 432–434. https://doi.org/10.1103/PhysRevLett.96.176101.

[46] A. Lerf, H. He, M. Forster, J. Klinowski, Structure of Graphite Oxide Revisited ǁ, J. Phys. Chem. B. 102 (1998) 4477–4482. https://doi.org/10.1021/jp9731821.

[47] W. Chih-Huang, Y.-F. Pan, Adsorption of a cationic dye (methylene blue) onto spent activated clay, J. Hazard. Mater. 144 (2007) 355–362. https://doi.org/10.1016/j.jhazmat.2006.09.097.

[48] D.W. Johnson, B. S.Coleman, K. Dobson, A manufacturing perspective on graphene dispersions, Curr. Opin. Colloid Interface Sci. 20 (2015) 367–382. https://doi.org/10.1016/j.cocis.2015.11.004.

[49] R.J. Hunter, Zeta Potential in Colloid Science, 1st ed., Oxford University Press, New York, 1988.

[50] J. Taha-Tijerina, D. Venkataramani, C.P. Aichele, C.S. Tiwary, J.E. Smay, A. Mathkar, P. Chang, P.M. Ajayan, Quantification of the particle size and stability of graphene oxide in a variety of solvents, Part. Part. Syst. Charact. 32 (2015) 334–339. https://doi.org/10.1002/ppsc.201400099.

[51] R.. Hunter, “Electro kinetics and zeta potential” in Foundations of Colloid Science, 2nd ed., Oxford University Press, New York, NY, 2001.

[52] S. Kashyap, S. Mishra, S.K. Behera, Aqueous Colloidal Stability of Graphene Oxide and Chemically Converted Graphene, J. Nanoparticles. 2014 (2014) 1–6. https://doi.org/10.1155/2014/640281.

[53] T. Szabo, P. Maroni, I. Szilagyi, Size-dependent aggregation of graphene oxide, Carbon N. Y. 160 (2020) 145–155. https://doi.org/10.1016/j.carbon.2020.01.022.

[54] J. Feng, J. Zhu, L. Wei, J. Li, W. Yan, Effect of hydroxyl group of carboxylic acids on the adsorption of Acid Red G and Methylene Blue on TiO2, Chem. Eng. Journa;L. 269 (2015) 316–322. https://doi.org/10.1016/j.cej.2015.01.109.

[55] L. Nie, K. Goh, Y. Wang, J. Lee, Y. Huang, H.E. Enis Karahan, K. Zhou, M.D. Guiver, T.H. Bae, Realizing small-flake graphene oxide membranes for ultrafast size-dependent organic solvent nanofiltration, Sci. Adv. 6 (2020) 1–13. https://doi.org/10.1126/sciadv.aaz9184.

[56] Y. Wei, Y. Zhang, X. Gao, Y. Yuan, B. Su, C. Gao, Declining flux and narrowing nanochannels under wrinkles of compacted graphene oxide nanofiltration membranes, Carbon N. Y. 108 (2016) 568–575. https://doi.org/10.1016/j.carbon.2016.07.056.